

Spectral Topological Data Analysis of Brain Signals

Anass B. El-Yaagoubi

Statistics Program

King Abdullah University of Science and Technology

Thuwal, Saudi Arabia

ANASS.BOURAKNA@KAUST.EDU.SA

Shuhao Jiao

Statistics Program

King Abdullah University of Science and Technology

Thuwal, Saudi Arabia

SHUHAO.JIAO@KAUST.EDU.SA

Moo K. Chung

Department of Biostatistics & Medical Informatics

University of Wisconsin–Madison

Madison, WI, USA

MKCHUNG@WISC.EDU

Hernando Ombao

Statistics Program

King Abdullah University of Science and Technology

Thuwal, Saudi Arabia

SHUHAO.JIAO@KAUST.EDU.SA

Editor: .

Abstract

Topological data analysis (TDA) has become a powerful approach over the last twenty years, mainly due to its ability to capture the shape and the geometry inherent in the data. Persistence homology, which is a particular tool in TDA, has been demonstrated to be successful in analyzing functional brain connectivity. One limitation of standard approaches is that they use arbitrarily chosen threshold values for analyzing connectivity matrices. To overcome this weakness, TDA provides a filtration of the weighted brain network across a range of threshold values. However, current analyses of the topological structure of functional brain connectivity primarily rely on overly simplistic connectivity measures, such as the Pearson correlation. These measures do not provide information about the specific oscillators that drive dependence within the brain network. Here, we develop a frequency-specific approach that utilizes coherence, a measure of dependence in the spectral domain, to evaluate the functional connectivity of the brain. Our approach, the spectral TDA (STDA), has the ability to capture more nuanced and detailed information about the underlying brain networks. The proposed STDA method leads to a novel topological summary, the spectral landscape, which is a 2D-generalization of the persistence landscape. Using the novel spectral landscape, we analyze the EEG brain connectivity of patients with attention deficit hyperactivity disorder (ADHD) and shed light on the frequency-specific differences in the topology of brain connectivity between the controls and ADHD patients.

Keywords: brain dependence, persistence landscape, spectral landscape, spectral topological data analysis, time series analysis, topological data analysis.

1. Introduction

Neuroscience aims to study and comprehend the fundamental brain function and mechanisms involved in the processing cognitive functions that memory, attention, and decision-making. Since the nineteenth century, neuroscientists continue to marvel at the complexity of the brain structural network. Over the years, advances in brain imaging technologies have enabled neuroscientists to observe the brain "in action" and thus have also uncovered the complexity of the functional brain network (Sporns et al. (2005), Park and Friston (2013)). These advances have resulted in a paradigm shift from the localization of brain processes (i.e., brain segregation) (Phillips et al. (1984), Zeki et al. (1991)) to the integration of brain activity (i.e., brain integration) (Giulio Tononi (1992), Friston (2011)). The goal of this paper is to develop a novel statistical approach to analyze and assess the presence and alterations of frequency-specific topological patterns in the connectivity of the brain. Frequency-specific TDA (or Spectral TDA) offers distinct advantages over coherence analysis and traditional time-frequency analysis. While coherence analysis provides frequency-specific pair-wise dependence measures (i.e., between two nodes in a network), TDA transcends these limitations by uncovering intricate topological patterns and relationships within the brain's functional network. The proposed STDA will not focus solely on pairwise connections but it will provide information about interactions that involve multiple channels and regions. Hence, the advantage of STDA is that it has the ability to uncover the complex interplay and organization of activity in the entire network. By exploring cluster formations, cycles, and holistic network properties within specific frequency bands, STDA provides a richer and more holistic perspective on cognitive processes and brain connectivity dynamics. Thus, our proposed STDA extends beyond traditional analyses, enhancing our understanding of the brain's intricate functional architecture.

The use of graph theory has been instrumental in gaining valuable insight, particularly in investigating brain networks—a network composed of nodes (brain regions) and dyadic edges (pairwise interactions between different brain regions) (Bassett and Bullmore (2006), den Heuvel et al. (2008), Bassett and Bullmore (2017), Sporns (2018)). Moreover, it has been a key tool that has aided neuroscientists in identifying patterns in the brain's functional connectivity, leading to a better understanding of the brain's structure, functional interconnection, and function. Albeit the human brain network is very complex (Bullmore and Sporns (2009), Sporns (2010)), graph theory has led to a better discrimination and understanding of the impact of various neurological disorders on brain connectivity (Caputi et al. (2021), Miraglia et al. (2022)). Usually, such graph theoretical approaches are built upon the analysis of network summaries, including metrics such as modularity (identification of communities within the network), centrality (measurement of a node's importance), node degree (count of connections each node has), and average shortest path (average length of the shortest paths between all pairs of nodes), among others (Simpson et al. (2013), BRA (2016)), after the weighted network of interest is thresholded. This approach faced extensive criticism in the literature due to its reliance on thresholding methods, which often result in arbitrarily oversimplified networks. This oversimplification introduces potential bias and can lead to a significant loss of valuable information. Despite the existence of heuristics to tackle the threshold selection problem (Langer et al. (2013), Bordier et al. (2017)), examples in the literature have shown that such oversimplified outputs can lead to erroneous

conclusions. For instance, in the study by Adamovich et al. (2022) (Adamovich et al. (2022)), the authors demonstrated that different threshold choices can lead to significant variations in the graph’s global connectivity when using various synchronization measures such as coherence. Consequently, the choice of these arbitrary and subjective thresholds could result in divergent study conclusions.

Instead of analyzing a single thresholded network composed of nodes (brain regions or channels) and dyadic edges (pairwise interactions between nodes), topological data analysis (TDA) considers higher-order interactions, providing a more comprehensive view of the entire network. This approach takes into account all connected nodes collectively, rather than focusing solely on pairwise connections. TDA approaches offer a significant advantage by considering all threshold levels, as illustrated in Figure 2, allowing the analysis of an increasing sequence of simplicial complexes, higher-order generalizations of graphs (refer to Figures 5 and 6). This approach is discussed in detail in works such as (Ghrist (2008) and Carlsson (2009)). Hence, TDA effectively addresses the thresholding challenge and has the capability to identify a broader range of topological dependence patterns within the data across various weight levels, including loops, cavities, and cliques. These patterns are visually demonstrated in brain networks in Figure 2 (Lee et al. (2012), Centeno et al. (2022), El-Yaagoubi et al. (2023)). While traditional methods primarily seek to compare the thresholded network structure, often focusing on summaries such as modularity and centrality (as illustrated in Figure 1), TDA provides a more comprehensive understanding of the network structure across various thresholding levels. Through TDA, we can discern which components of the structure persist across a wide range of thresholds, signifying their robustness, and contrast this with components that emerge briefly before dissipating (‘dying’) soon after their inception. This nuanced view of the network’s evolution is exemplified in Figure 2.

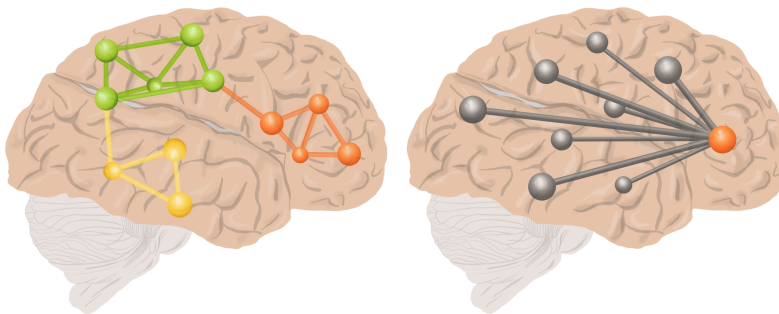


Figure 1: An Example of two networks. Left: emphasizing high modularity. Right: emphasizing high centrality.

Despite the initial success of TDA in analyzing brain networks (Caputi et al. (2021)), the current approaches often rely on using correlation-based connectivity measures (Lee et al. (2012), Giusti et al. (2015)), where an edge is said to exist between a pair of nodes when the absolute value of the pairwise correlation exceeds some threshold. While useful as a first step for studying brain functional connectivity, simple correlations between brain regions

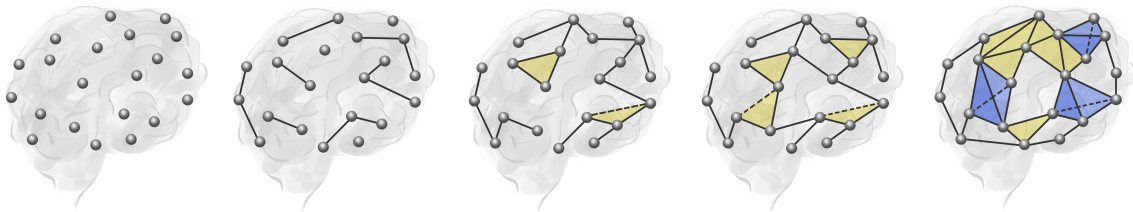


Figure 2: Illustration of the TDA approach to network analysis, encompassing multiple threshold values and forming a nested sequence of networks.

presents several limitations. Since brain signals have been shown to display frequency-specific synchronization, the use of simple correlations can result in inadequate assessment of brain dependence. This can lead to a loss of power to detect changes in the connectivity structure, as well as a lack of sensitivity to possible variations in connectivity across different frequency bands, potentially overlooking valuable information within the data.

Brain signals are observations of complex neurophysiological processes that are recorded using different modalities. One of the most common and easily accessible modalities is electroencephalogram (EEG) signals, which measure brain electrical activity. One of the primary advantages of EEG is its high temporal resolution, typically at 1000 Hertz (Hz) (Nunez and Srinivasan (2006)). But EEGs are generally prone to artifacts such as eye-blinking, eye movement, and muscle contractions, but these can be removed via pre-processing techniques. These signals are subject to structural filtering due to the cerebrospinal fluid, skull, skin and hair. EEG signals are often analyzed in the frequency domain. The first step involves estimating the spectrum at each channel to identify the dominant oscillation frequencies contributing to the signal. In the second step, we examine the interdependence between pairs of brain network channels. For an in-depth exploration of spectral dependence, refer to (Ombao and Pinto (2022)). When two brain signals from different channels display a high correlation, the subsequent procedure involves pinpointing the primary frequency oscillations contributing to this correlation. Consequently, coherence is an ideal choice for measuring frequency-specific dependence as the relative synchronization between various brain regions (or brain channels) (Shaw (1984), Ombao et al. (2005), ?, Bowyer (2016), Ombao and Pinto (2022)). In Ombao and Pinto (2022), coherence is motivated as follows. An observed EEG signal comprises various frequency-specific random oscillations. Coherence between two brain regions within a specific frequency band can be understood as the squared correlation between their filtered signals at that frequency (refer to Figure 3). In practice, when there are lead-lag relationships between the oscillations, the filtered signals are time-shifted to maximize the squared cross-correlation for an illustrative example).

Therefore, analyzing the topology of dependence in brain signals without considering their spectral properties may result in incomplete information and characterization of dependence. In this paper, we will develop the STDA method which will serve as a additional tool in the TDA toolbox.

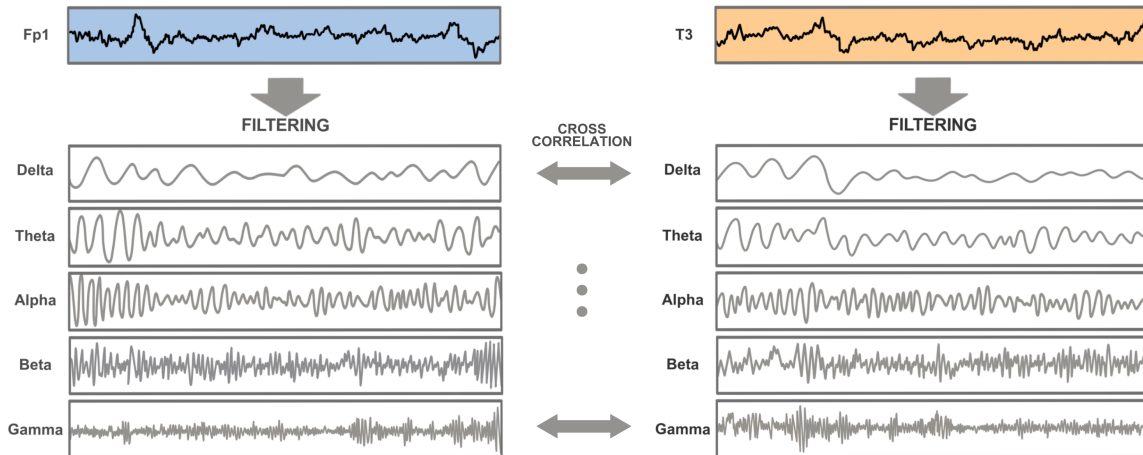


Figure 3: Brain signal decomposition into different frequency bands: δ (0.5Hz to 4Hz), θ (4Hz to 8Hz), α (8Hz to 12Hz), β (12Hz to 30Hz), and γ (30Hz to 50Hz). Coherence within a specific frequency band can be interpreted as the squared frequency-specific cross-correlation.

Motivated by the difficulties discussed above, we propose a novel method that leverages coherence to generate a frequency-specific topological summary of healthy and ADHD brain dependence structure. This approach allows us to capture unique patterns of brain connectivity that vary across different frequency bands, providing a more comprehensive understanding of neural interactions. In Figure 4, we provide an illustrative example that showcases our approach’s effectiveness in detecting topological patterns, emphasizing the superiority of TDA on coherence over TDA on correlation. While TDA on coherence excels in identifying topological patterns, particularly when connectivity exhibits variations across different frequencies, TDA on correlation, with its simplified structure, will fail to do so.

One major advancement of this topological summary is that it can effectively distinguish between the topological structure of different groups across various frequency bands. Section 2 presents a brief overview of the founding concepts of persistence homology. Section 3 presents spectral persistence homology and introduces a novel topological summary named spectral landscape (SL) with its main statistical properties. Furthermore, we develop a functional testing procedure based on the SL to assess the frequency-specific topological differences between two groups of multivariate brain signals. Section 4 focuses on a simulation study demonstrating the proposed summary’s ability to detect topological differences and dissimilarities between two dependence structures across different frequencies. In Section 5, we use SLs to analyze and compare the frequency-specific dependence structure in EEG signals of two groups; ADHD and healthy controls. Our approach provides statistically significant evidence for frequency-specific alteration in the topology of brain connectivity during a visual attention task in ADHD subjects.

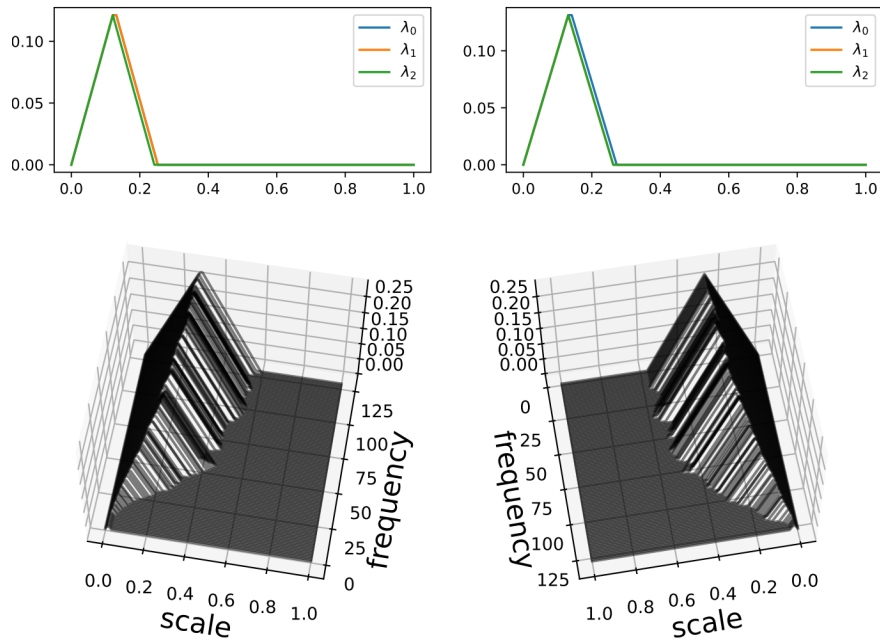


Figure 4: Example: Comparing TDA on Coherence vs. TDA on Correlation. Top: Traditional Persistence Landscapes (correlation-based) for low (Left) and high (Right) frequencies, which fail to distinguish the two examples. Bottom: Novel Spectral Landscapes (coherence-based) offer richer summaries that distinguish the two examples.

2. Persistence homology and topological summaries

Topological data analysis (TDA) has witnessed many significant advances over the last twenty years that aim to unravel and provide insight into the "shape" of the data (Edelsbrunner et al. (2002), Carlsson et al. (2004), Ghrist (2008), Edelsbrunner and Harer (2008), Carlsson (2009), Bubenik (2015)). These TDA tools are designed to extract the "global" topological and geometrical features present in high-dimensional data, which are not directly accessible using other classical techniques in graph theory which provide a more "local" type of analysis (e.g., examining pairwise edges rather a collection of edges in the entire network).

In the next subsections, we provide a concise review of key concepts in persistence homology, as well as an overview of some fundamental TDA summaries. We then introduce our novel Spectral TDA (STDA) approach — which is generalization of classical TDA on correlations. We then present a rigorous testing framework designed to identify topological differences in brain dependence structures between different groups across various frequency bands. The proposed STDA is grounded in robust theoretical foundations, offering valuable asymptotic insights.

2.1 Persistence homology of weighted networks

The application of TDA to time series analysis is usually made by transforming the data into a cloud of points via a time delay embedding or sliding window procedure (Perea and Harer (2015)). The final goal is to detect the system’s features from a dynamic systems point of view (Gholizadeh and Zadrozny (2018)). However, it is not always possible to directly identify topological patterns in the ”shape” of the data. In particular, working with brain signals such as EEGs, there is no apparent structure or trend in the time domain since these are often viewed as zero-mean processes (El-Yaagoubi et al. (2023), Ombao and Pinto (2022), Ombao et al. (2005), Park et al. (2014), Fiecas and Ombao (2016)). Therefore, it is common in TDA literature to transform the brain signals into a dependence network, which captures the inter-dependencies and interactions among different brain regions (Bullmore and Sporns (2009), Sporns (2018)) and analyze the topological structure of brain connectivity using correlations, for instance.

In the following we denote by $X_i(t)$ the observed brain process from location $i \in V$ and time $t \in \{1, \dots, T\}$, where $V = \{1, \dots, P\}$ is the set of all P locations on the brain. Let $G = (V, W)$ be the weighted brain connectivity network with given P locations and dependence weights $W_{i,j} = \text{Dep}(X_i, X_j)$. Usually, dependence is measured by correlations, and a dissimilarity measure between brain channels is defined as $d_X(X_i, X_j) = 1 - \text{corr}(X_i, X_j)$, where d_X quantifies the dissimilarity or the gap between brain signals X_i and X_j . It is important to note that this measure does not satisfy the triangle inequality property.

Define the binary network filtration, denoted $B(X, \epsilon)$, to be the thresholded networks whose nodes are the P locations and whose edges are stated to be present if the distance d_X between a pair of nodes X_i and X_j is less than the threshold ϵ , see example in Figure 7. The study of such filtration $\{B(X, \epsilon), \epsilon > 0\}$, has the advantage of not being limited to one arbitrary threshold ϵ but instead, it considers all threshold values (Lee et al. (2012)).

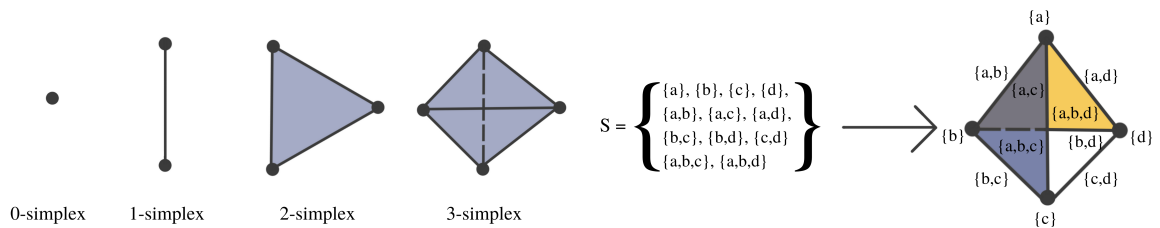


Figure 5: Illustration of the first three simplices.

Figure 6: Example of a simplicial complex.

In geometry, a simplex generalizes concepts like edges, triangles, and tetrahedra into higher dimensions. In Figure 5, a 0-simplex represents a node or point, a 1-simplex is an edge in a graph, and a 2-simplex forms a triangle, extending into higher dimensions. A simplicial complex, shown in Figure 6, is constructed by combining simplices. For precise definitions, please refer to (Munkres (1984), Merkulov (2003)). Therefore, instead of considering the filtration of binary edges in $B(X, \epsilon), \epsilon > 0$, we explore the more intricate structure known as the Rips filtration, denoted by $R(X, \epsilon), \epsilon > 0$. For a given ϵ , $R(X, \epsilon)$ forms a simplicial

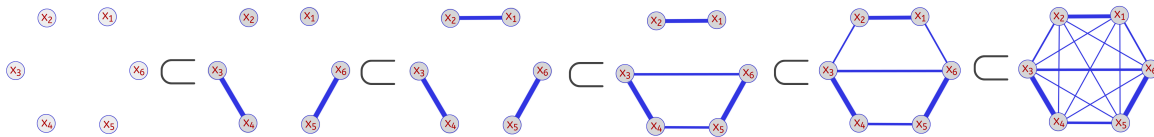


Figure 7: Examples of a dependence network threshold filtration.

complex where k -simplices consist of $(k + 1)$ nodes within an ϵ -distance of each other (refer to Figure 2 and 3 in Ghrist (2008)). It's important to note that for any threshold value, the binary network represents a special case of the Rips complex, i.e., $B(X, \epsilon) \subset R(X, \epsilon)$, with $B(X, \epsilon)$ containing only 0- and 1-simplices. Henceforth, we denote the Rips complex as \mathcal{X}_ϵ .

2.2 Topological summaries

The Rips filtration, illustrated in Figure 7, serves as a powerful data structure that encapsulates crucial topological insights within the original data. Unlike traditional methods that often focus solely on dyadic relations between pairs of brain signals, the Rips filtration offers a more comprehensive perspective. It not only accounts for these pairwise interactions but also explores higher-dimensional combinations, uncovering complex network patterns that are otherwise overlooked. This multi-dimensional approach enhances our ability to capture intricate dependencies within the data, providing a richer understanding of brain connectivity. Although conventional techniques, such as correlation analysis or spectral analysis based on dyadic relations, offer valuable insights, they are limited in their capacity to unveil the full spectrum of connectivity patterns present in complex systems like the brain. The Rips filtration, by contrast, empowers us to unearth and analyze these intricate relationships, making it a valuable tool for the study of brain networks.

While Rips filtrations form the foundational framework for our network topology analysis, Betti numbers, as depicted in Figure 8, serve as the invaluable lenses through which we gain insight into the intricate topological properties of networks. Consequently, by examining the scales at which Betti numbers change within the Rips filtration of a given weighted network, we can extract a diverse array of valuable topological summaries. Betti numbers, characterizing the network's underlying topology, allow us to delve deeper into the network's structure and understand its evolving connectivity patterns at various scales. Therefore, many tools and summaries have been proposed in the TDA literature to analyze the shape of the data through Rips filtration (Carlsson et al. (2004), Edelsbrunner and Harer (2008), Ghrist (2008), Bubenik (2015)). Transitioning from the barcodes, which encode the lifetimes of topological features, to the persistence landscape and, finally, to the persistence diagrams, as illustrated in Figure 9, these topological summaries aim to analyze the birth and death times (appearance and disappearance) of topological structures of various dimensions, such as connected components (0-dimensions), non-oriented cycles (1-dimensions), cavities (2-dimensions), etc. in a convenient manner. The times or scales ϵ at which the Betti numbers of the Rips filtration change will characterize the appearance and disappearance of various topological features. Thus, by analyzing the distribution of such scale stamps, we can discover interesting properties in the underlying brain dependence.

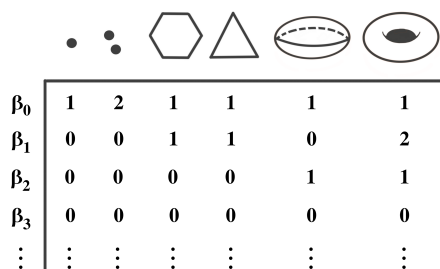


Figure 8: Examples of topological objects with their corresponding Betti numbers.

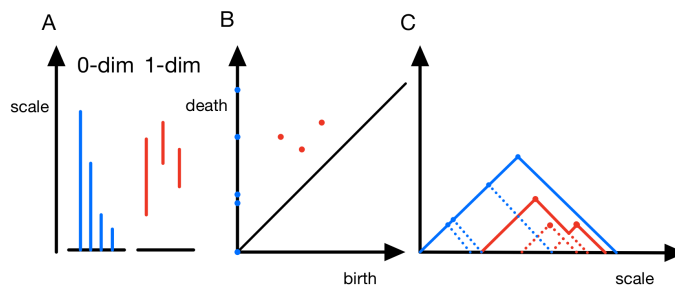


Figure 9: (A) Example of a barcode; (B) the corresponding persistence diagram; (C) the corresponding persistence landscape. The 0-dim. components are represented in blue; the 1-dim. components are represented in red.

3. Spectral persistence homology

As already noted, the use of correlations to measure brain dependence is extremely simplistic and thus presents several limitations. Brain signals such as electroencephalograms have high temporal resolution and are observations of complex underlying neurophysiological processes. An alternative to cross-correlations is coherence which measures brain dependence as the relative synchronization between various brain regions (or brain channels). Coherence enables neuroscientists to identify the specific oscillatory activity (or activities) shared between signals/channels in a brain network (Shaw (1984), Ombao and Van Bellegem (2008), Bowyer (2016), Ombao and Pinto (2022)).

3.1 Coherence-based simplicial complexes

In neuroscience, the study of brain connectivity is typically categorized into three distinct domains, namely, structural, functional, and effective brain connectivity (Park and Friston (2013), Babaeeghazvini et al. (2021)). The first category, aims at understanding the brain's anatomical connections that link various cortical and subcortical regions. The second category aims at understanding how the human brain drives cognitive function by integrating electric information across multiple segregated regions by studying the statistical interdependencies between different brain signals without taking into account the information on directionality. The third category, effective brain connectivity, studies the directed influence of one region on another and how this influence affects the brain's overall functioning.

Since the 1960s, coherence has been a valuable tool for evaluating functional connectivity, particularly in the context of assessing synchronized neural activity using EEG sensors (Shaw (1984), Bowyer (2016)). To understand coherence, we'll start with a fundamental concept called the Cramér representation.

a simplicial complex, where $\mathcal{X}_{\epsilon_1}(\omega)$ is the first frequency-specific simplicial complex (single nodes) and $\mathcal{X}_{\epsilon_n}(\omega)$ is the last frequency-specific simplicial complex (all nodes connected, i.e., a clique of size n). Note that for P nodes (brain locations) there are at most $\binom{P}{2} = \frac{P \times (P-1)}{2}$ strictly different pairwise distances. Thus, there are at most $\binom{P}{2}$ simplicial complexes in this Rips filtration for every frequency. However, the total number of simplicial complexes is doubly exponential in P , i.e., in $\mathcal{O}(2^{2^{c \times P}})$. This used to be known as the Kalai conjecture but was recently proved in (Newman (2022)). For a thorough explanation of constructing Rips filtrations based on metric space refer the reader to Hausmann (2016).

Given a frequency-specific filtration $\mathcal{X}(\omega) = \{\mathcal{X}_\epsilon(\omega), \epsilon \in [0, 1]\}$, the homology group $H_k(\mathcal{X}_\epsilon, \omega)$ of $\mathcal{X}(\omega)$ changes as the threshold ϵ increases: new connected components can appear, others can merge, non-oriented cycles or loops and cavities can be formed or destroyed, and so on. By tracking the birth and death thresholds and encoding them as a set of intervals (ϵ_b, ϵ_d) , we obtain a barcode. Equivalently, the (ϵ_b, ϵ_d) pairs can be represented as point coordinates in a \mathbb{R}^2 ; this is known as a persistence diagram (dgm), see Figure 9.

3.2 A novel topological summary: The Spectral landscapes

In topological data analysis, the absence of rigorous statistical inference methods for many summaries poses a significant challenge, particularly when the goal is to compare populations of barcodes or persistence diagrams (e.g., disease population vs healthy control population). This challenge arises due to the inherent difficulty in defining a "distribution" of barcodes or persistence diagrams. Consequently, there will be the challenge of defining and computing the population mean or "center" of the distribution of barcodes or persistence diagrams. Additionally, it will be a challenge to derive and compute a reliable "confidence sets" of barcodes and persistence diagrams.

To address these challenges, we will develop an inferential procedure that can flexibly lend to formal statistical inference. In particular, we will derive estimates of (i.) population-specific and (ii.) subject-specific summaries, which makes a two-stage analysis and a two-sample hypothesis testing possible. Here, rather than using persistence diagrams, we will use alternatives such as the persistence landscapes (in Bubenik (2015)) or persistence images (in Adams et al. (2017)).

Unlike traditional approaches that analyze one brain connectivity network at a time, our frequency-specific approach based on coherence offers a distinct advantage. It empowers neuroscientists to simultaneously investigate multiple networks, thereby extending the concept of simplicial complexes into the frequency domain. Therefore, we introduce the spectral landscape, a novel frequency-specific generalization of the persistence landscape. Denote $dgm_k(\omega)$ to be the frequency-specific persistence diagram for the k -th homology group $H_k(\mathcal{X}_\epsilon, \omega)$. Define the corresponding ℓ -th spectral landscape $\Lambda_{k,\ell}$ to be

Definition 1 (Spectral landscape)

$$\lambda_p(s) = \begin{cases} s - b, & s \in [b, \frac{b+d}{2}), \\ d - s, & s \in [\frac{b+d}{2}, d), \\ 0 & \text{otherwise,} \end{cases} \quad (6)$$

$$\Lambda_{k,\ell}(s, \omega) = \ell \max_{p \in dgm_k(\omega)} \lambda_p(s). \quad (7)$$

For every frequency ω , $\Lambda_{k,\ell}(\cdot, \omega)$ is a persistence landscape. Since the distance function d_x takes values in $[0, 1]$, the (birth, death) pairs also will take values $[0, 1]$. Consequently, the spectral landscape has the following properties directly following from Definition 1:

1. $0 \leq \Lambda_{k,\ell}(s, \omega) \leq \frac{1}{2}$,
2. $\Lambda_{k,\ell}(s, \omega) \geq \Lambda_{k,\ell+1}(s, \omega)$,
3. $\Lambda_{k,\ell}$ is 1-Lipschitz in s .

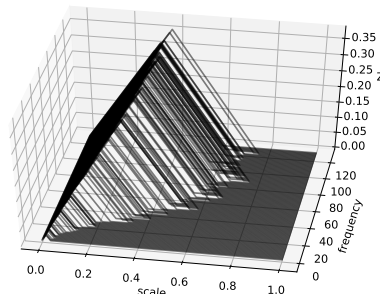


Figure 10: Example of a spectral landscape Λ_0 corresponding to the 0-dimensional homology group.

In the following, we only consider the first level ($\ell = 1$), which corresponds to the most persistent features, and denote the corresponding spectral landscape Λ_k , as displayed in Figure 10.

3.3 Convergence of spectral landscapes

In neuroscience experiments, brain signals are often collected from several participants ($i = 1, \dots, n$). Then the participant-specific coherence matrix is estimated: $\{\widehat{\mathcal{C}}_i(\omega) \mid \omega \in [0, \frac{1}{2}]\}$. From this frequency-specific object, we build our participant-specific topological summaries. Therefore, we can consider spectral landscapes $\Lambda_{k,i}$ as Borel random variables defined on some underlying probability space $(\Omega, \mathcal{F}, \mathbb{P})$, with values in the separable Banach space L^p with the usual L^p -norm for some $1 \leq p < \infty$, i.e., $\Lambda_k = V(\xi)$. Following the approach in (Bubenik (2015)), we state the strong law of large numbers and the central limit theorem for sequences of Borel random variables defined on Banach spaces and apply these results to the spectral landscape.

Consider the sample average $\bar{V}^n = \frac{1}{n} \sum_{i=1}^n V_i$ of n independent copies V_i of a Borel random variable V defined on a Banach space. We then state the following convergence theorems (for details, see Hoffmann-Jørgensen and Pisier (1976) and Ledoux and Talagrand (2011)).

Theorem 2 (Strong Law of Large Numbers)

$$\bar{V}^n \rightarrow \mathbb{E}(V) \quad \text{almost surely if and only if } \mathbb{E}(\|V\|) < \infty.$$

Theorem 3 (Central Limit Theorem)

$$\text{If } \mathbb{E}(V) = 0 \text{ and } \mathbb{E}(\|V\|^2) < \infty \text{ then } \sqrt{n} \bar{V}^n \text{ converges weakly to } G,$$

where G is a Gaussian random variable with zero-mean and the same covariance as V .

For a given homology dimension k , consider a sequence of n spectral landscapes $\Lambda_{k,i}$ as Banach random variables such that $\mathbb{E}(\Lambda_{k,i}) = \mu_k$. By applying Theorem 2 and Theorem 3 to the sample average spectral landscape $\bar{\Lambda}_k^n(s, \omega) = \frac{1}{n} \sum_{i=1}^n \Lambda_{k,i}(s, \omega)$, we obtain the following two theorems for spectral landscapes:

Theorem 4 (Strong Law of Large Numbers for Spectral Landscapes)

$$\bar{\Lambda}_k^n \rightarrow \mu_k \quad \text{almost surely if and only if } \mathbb{E}(\|\Lambda_{k,i}\|) < \infty.$$

Theorem 5 (Central Limit Theorem for spectral landscapes)

$$\text{If } \mathbb{E}(\|\Lambda_{k,i}\|^2) < \infty \text{ then } \sqrt{n} [\bar{\Lambda}_k^n - \mu_k] \text{ converges weakly to } G,$$

where G is a Gaussian random variable with 0-mean and has the same covariance as $\Lambda_{k,i}$.

The previous results are the foundations for building confidence regions for spectral landscapes and for deriving asymptotic properties of various transformations of such summaries, which will be developed in the next subsection.

3.4 A novel testing framework based on frequency-specific topological differences

Spectral landscapes play a crucial role in drawing inferences about the topology of frequency-specific dependence in a brain network for two populations of interest (e.g., control population vs. disease population), across the entire frequency range. It is possible that there are differences in the topology of brain signals only at low frequencies, but these differences might be negligible for brain signals at high frequencies. Spectral landscapes allow neuroscientists a comprehensive exploration of these variations, providing valuable insights into the frequency-specific patterns of brain connectivity. We will develop the following functional testing framework.

Our proposed approach will be applied for every homology dimension k , but we drop the subscript k for simplicity. Consider a set of spectral landscapes Λ_i , that can be viewed as a set of two-variate functions, i.e., $\Lambda_i : S \times \Omega \rightarrow \mathbb{R}$, where $S = [0, 1]$ is the distance range and $\Omega = [0, \frac{1}{2}]$ is the frequency range. Let Π_1 denote the control group, and Π_2 denote the disease group (e.g., the group of ADHD subjects), and assume that the spectral landscapes have a population mean function and a participant-specific deviation from the mean which is expressed in the following model:

$$\Lambda_i(s, \omega) = \begin{cases} \mu_1(s, \omega) + \mathcal{E}_i(s, \omega), & i \in \Pi_1, \\ \mu_2(s, \omega) + \mathcal{E}_i(s, \omega), & i \in \Pi_2. \end{cases}$$

Here the "error" functions $\mathcal{E}_i(s, \omega)$ are assumed to be independent and identically distributed across i with mean zero and finite second moments, these functions are intended to account for (a.) variation of the brain topology across members of the same population; and (b.) estimation error within each participant. The covariance functions of $\mathcal{E}_i(s, \omega)$ are defined as:

$$\Gamma_1(s_1, \omega_1, s_2, \omega_2) = E\{(\Lambda_i - \mu_1)(s_1, \omega_1)(\Lambda_i - \mu_1)(s_2, \omega_2)\}, \quad \text{for } i \in \Pi_1, \quad (8)$$

$$\Gamma_2(s_1, \omega_1, s_2, \omega_2) = E\{(\Lambda_i - \mu_2)(s_1, \omega_1)(\Lambda_i - \mu_2)(s_2, \omega_2)\}, \quad \text{for } i \in \Pi_2. \quad (9)$$

In order to test for topological differences in the dependence structure between the two groups for some frequency band Ω_ℓ we define the following null hypothesis:

$$H_0: \mu_1(s, \omega) = \mu_2(s, \omega) \text{ for all } s \in S, \omega \in \Omega_\ell \subset \Omega, \quad (10)$$

To formulate the testing procedure for the null hypothesis H_0 against the alternative that H_0 is false, we draw a random sample of sample sizes N_1 and N_2 from each of the two populations, respectively. In this context, we are interested in the scenario where the ratio $N_1/(N_1 + N_2)$ converges to a finite value c with $0 < c < 1$ as both N_1 and N_2 tend to infinity. Under the null hypothesis H_0 , and assuming that \mathcal{E}_i have finite second moments, we can establish the following convergence theorem.

Theorem 6 (STDA test statistic)

$$T_{N_1, N_2}^{\Omega_\ell} = \frac{N_1 N_2}{N_1 + N_2} \int_{S \times \Omega_\ell} (\hat{\mu}_1 - \hat{\mu}_2)^2(s, \omega) ds d\omega \xrightarrow{d} \int_{S \times \Omega_\ell} G^2(s, \omega) ds d\omega,$$

where

$$\hat{\mu}_1(s, \omega) = \frac{1}{N_1} \sum_{i \in \Pi_1} \Lambda_i(s, \omega), \quad \hat{\mu}_2(s, \omega) = \frac{1}{N_2} \sum_{i \in \Pi_2} \Lambda_i(s, \omega),$$

and G is a Gaussian process with zero-mean and covariance Γ , such that:

$$\Gamma(s_1, \omega_1, s_2, \omega_2) = (1 - c) \Gamma_1(s_1, \omega_1, s_2, \omega_2) + c \Gamma_2(s_1, \omega_1, s_2, \omega_2). \quad (11)$$

Proof Applying Theorem 5 to the mean spectral landscapes for both groups yields:

$$\sqrt{N_1} \{ \hat{\mu}_1 - \mu_1 \}(s, \omega) \xrightarrow{d} G_1(s, \omega), \quad (12)$$

$$\sqrt{N_2} \{ \hat{\mu}_2 - \mu_2 \}(s, \omega) \xrightarrow{d} G_2(s, \omega), \quad (13)$$

where G_1 and G_2 are, respectively, two independent Gaussian processes with mean zero and covariance Γ_1 and Γ_2 respectively as defined in Equations 8 and 9. Assuming $\mu_1 = \mu_2$ (i.e., under H_0), the test statistic $T_{N_1, N_2}^{\Omega_\ell}$ can be expressed as follows:

$$\begin{aligned} T_{N_1, N_2}^{\Omega_\ell} &= \frac{N_1 N_2}{N_1 + N_2} \int_{S \times \Omega_\ell} (\hat{\mu}_1 - \hat{\mu}_2)^2(s, \omega) ds d\omega, \\ &= \int_{S \times \Omega_\ell} \left\{ \sqrt{\frac{N_2}{N_1 + N_2}} \sqrt{N_1} (\hat{\mu}_1 - \mu_1) - \sqrt{\frac{N_1}{N_1 + N_2}} \sqrt{N_2} (\hat{\mu}_2 - \mu_2) \right\}^2(s, \omega) ds d\omega, \end{aligned}$$

using Equations 12 and 13 with the dominated convergence theorem yields:

$$\begin{aligned} T_{N_1, N_2}^{\Omega_\ell} &\xrightarrow{d} \int_{S \times \Omega_\ell} \left\{ \sqrt{1 - c} G_1 - \sqrt{c} G_2 \right\}^2(s, \omega) ds d\omega, \\ &= \int_{S \times \Omega_\ell} G^2(s, \omega) ds d\omega, \end{aligned}$$

where $G(s, \omega) = \sqrt{1 - c} G_1(s, \omega) - \sqrt{c} G_2(s, \omega)$, which is the Gaussian process with zero-mean and covariance $\Gamma = (1 - c) \Gamma_1 + c \Gamma_2$. More details can be found in (Horváth and

Kokoszka (2012)). ■

In practice, the quantities c , $\Gamma_1(s_1, \omega_1, s_2, \omega_2)$ and $\Gamma_2(s_1, \omega_1, s_2, \omega_2)$ are typically unknown, and are estimated by $\hat{c} = N_1/(N_1 + N_2)$ and

$$\begin{aligned}\hat{\Gamma}_1(s_1, \omega_1, s_2, \omega_2) &= \frac{1}{N_1} \sum_{i \in \Pi_1} \{\Lambda_i - \hat{\mu}_1\}(s_1, \omega_1) \{\Lambda_i - \hat{\mu}_1\}(s_2, \omega_2), \\ \hat{\Gamma}_2(s_1, \omega_1, s_2, \omega_2) &= \frac{1}{N_2} \sum_{i \in \Pi_2} \{\Lambda_i - \hat{\mu}_2\}(s_1, \omega_1) \{\Lambda_i - \hat{\mu}_2\}(s_2, \omega_2).\end{aligned}$$

While Theorem 6 is an important result, it remains of little practical importance to conducting statistical tests if we cannot compute the theoretical quantiles of the reference distribution. To accomplish this goal, we can express the reference distribution in a simpler form, as in Equation 15. The application of Karhunen-Loève theorem to the Gaussian process $G(s, \omega)$, provides us with the following decomposition:

$$G(s, \omega) = \sum_{d=1}^{\infty} \lambda_d^{1/2} N_d \nu_d(s, \omega),$$

where $\{N_d: d \geq 1\}$ are *i.i.d.* standard normal random variables, and $\{\lambda_d: d \geq 1\}$ and $\{\nu_d: d \geq 1\}$ are the set of eigenvalues and (orthonormal) eigenfunctions of the covariance Γ . Based on this decomposition, it can be shown that the integral form of the reference distribution in 6 can be expressed as an infinite series of weighted chi-square random variables:

$$\int_{\mathcal{S} \times \Omega_\ell} G^2(s, \omega) ds d\omega = \sum_{d=1}^{\infty} \lambda_d N_d^2. \quad (14)$$

In the literature, the test statistic $T_{N_1, N_2}^{\Omega_\ell}$ is compared with the quantiles of an approximate reference distribution (under the null hypothesis H_0) which is a truncated version of the true reference distribution.

$$T_{N_1, N_2}^{\Omega_\ell} \xrightarrow{d} \sum_{d=1}^{\infty} \lambda_d N_d^2 \sim \sum_{d=1}^D \lambda_d N_d^2. \quad (15)$$

According to the asymptotic results discussed above, as long as the truncation parameter D is sufficiently large, this approximation will provide reliable results since the eigenvalues are absolutely summable. To estimate the eigenvalues $\{\lambda_d: d = 1, \dots, D\}$ we decompose the estimated covariance of the Gaussian process in Equation 16:

$$\hat{\Gamma}(s_1, \omega_1, s_2, \omega_2) = \frac{N_2}{N_1 + N_2} \hat{\Gamma}_1(s_1, \omega_1, s_2, \omega_2) + \frac{N_1}{N_1 + N_2} \hat{\Gamma}_2(s_1, \omega_1, s_2, \omega_2). \quad (16)$$

Since the rank of the estimated covariance $\hat{\Gamma}$ in Equation 16 is at most $N_1 + N_2$, taking $D = N_1 + N_2$ does not result in a loss of information, as $\lambda_d = 0, \forall d > D$. It is, therefore, possible to truncate the series in Equation 14 without altering the reference distribution.

4. Simulation study

In this section we investigate, through numerical experiments, the ability of spectral landscapes to capture topological patterns within the dependence structure of multivariate time series and across different frequency bands. To facilitate this investigation, we propose four distinct settings with four dependence patterns which are shown in Figure 12. Here, multivariate electroencephalograms (EEG) signals with a specified dependence structure will be generated as mixtures of random oscillations across all frequencies. To capture specified behavior of these oscillations (as characterized by the location and bandwidth of the spectral peak), we will use the first-order and second-order autoregressive (AR) processes (see Figure 11). This idea of generating EEGs as mixtures of AR processes were employed in Gao et al. (2020) and Granados-Garcia et al. (2022).

The first step is to estimate the coherence structure from the multivariate signals originating from these four settings. Second, using the coherence based distance function, we build the corresponding spectral landscapes. Subsequently, leveraging our spectral approach, we conduct a pairwise testing procedure for the four groups, focusing on the low frequency range of 0 – 12 Hertz (which corresponds to the delta-theta-alpha range) and middle-range beta of 12 – 27 Hertz, and the high frequency bands 27 – 50 Hertz (which corresponds to the high-beta to gamma range), for the 0-dimensional and 1-dimensional homology structures.

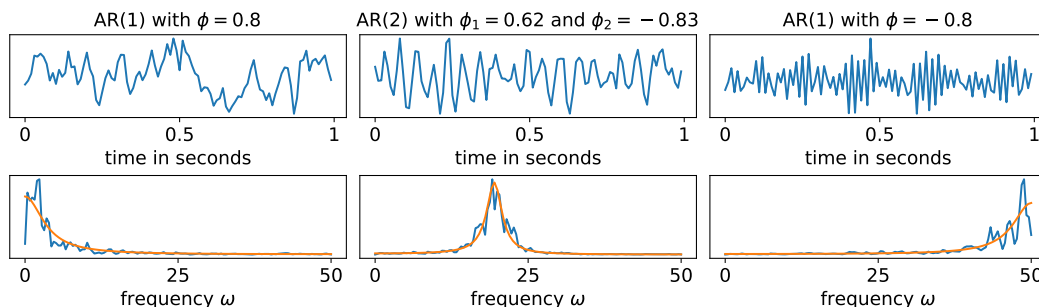


Figure 11: Top: Three realizations of autoregressive processes. Bottom: The corresponding power spectra. True spectrum in orange and periodogram or spectral estimates in blue.

4.1 Simulation settings

To investigate the ability of spectral landscapes to capture topological patterns within the dependence structure of multivariate time series across different frequency bands, we will study the following four settings based on mixtures of AR(1) and AR(2) processes:

1. Setting 1: Fully connected, low-frequency band.
2. Setting 2: Fully connected, high-frequency band.
3. Setting 3: Cyclic connectivity, middle/beta frequency band.

4. Setting 4: Random connectivity, middle/beta frequency band.

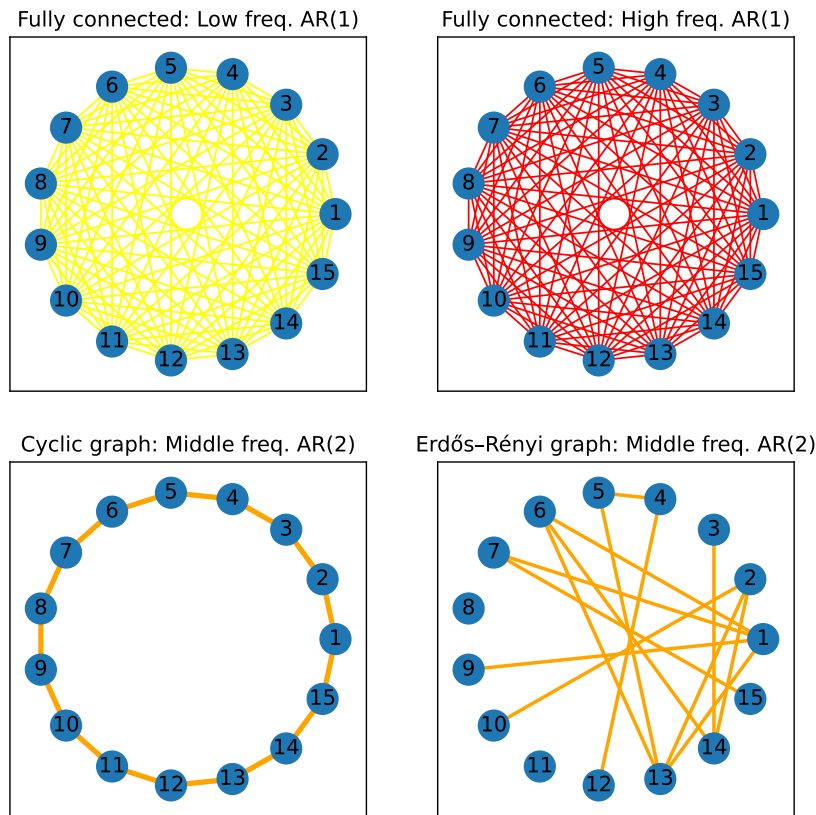


Figure 12: Four simulation settings. Top row, represents the fully connected structure based on AR(1) process. Bottom row represents cyclic and random dependence pattern. **Yellow** edges represent dependence at low frequency band, **red** edges represent dependence at high frequency band, and **orange** edges represent dependence at beta frequency band.

For each scenario above, we simulated $n = 20$ P -dimensional multivariate time series, with $T = 1000$ observations. In Settings 1 and 2, we used a latent AR(1) process to generate the fully connected dependence structure. For example, $X_p(t) = Z_L(t) + \epsilon_p(t)$ with $Z_L(t)$ representing a **low frequency** AR(1) process with $\rho = 0.8$, and $Y_p(t) = Z_H(t) + \epsilon_p(t)$ with $Z_H(t)$ representing a **high frequency** AR(1) process with $\rho = -0.8$, as can be seen in Figure 11. In Settings 3 and 4, we simulated mixtures of AR(2) processes concentrated around the beta (12-27Hz) frequency band, see Figure 11. In order to generate a random dependence pattern with a similar number of edges, we sampled from an Erdős-Rényi graph with edge probability $p_E = \frac{2}{P-1}$, where P is the dimension of the multivariate time series. In doing so we guarantee that, on average, the cyclic network and the random network will have the same number of edges P and same node degree 2 for all nodes. We followed the procedure in (El-Yaagoubi et al. (2022)) to generate the mixtures of AR(2) processes with the topological pattern defined in Figure 12.

4.2 Estimation of the spectral landscapes

Classical TDA techniques are able to capture the topological information present in a weighted dependence network. However, this information is not frequency-specific, hence, conclusions may lack specificity and interpretability (Ombao and Pinto (2022)). Brain functional networks may have connectivity pattern that changes between frequency bands (see, e.g., Shaw (1984), Wang et al. (2016)).

After simulating the data as explained in Section 4.1, we first estimated the coherence matrix using a smoothed periodogram approach, then applied our STDA approach as presented in Sections 3.1 and 3.2. In Figures 13 and 14, we report the group average spectral landscapes for Settings 1–4, and for both homology dimensions 0 and 1.

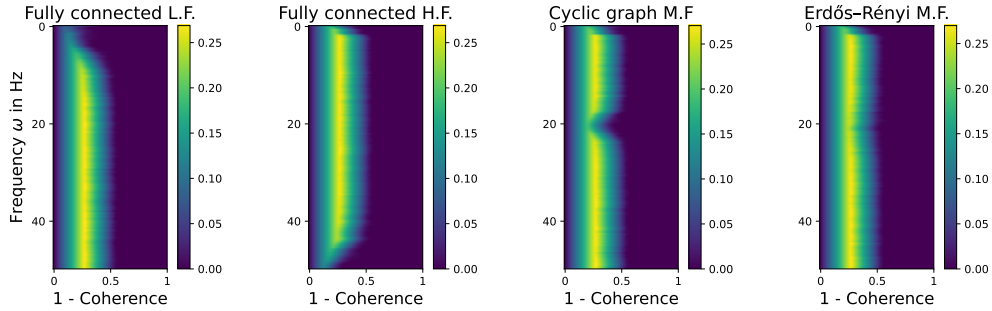


Figure 13: Left to right: Spectral landscape functions for settings 1–4 for the 0-dimensional homology.

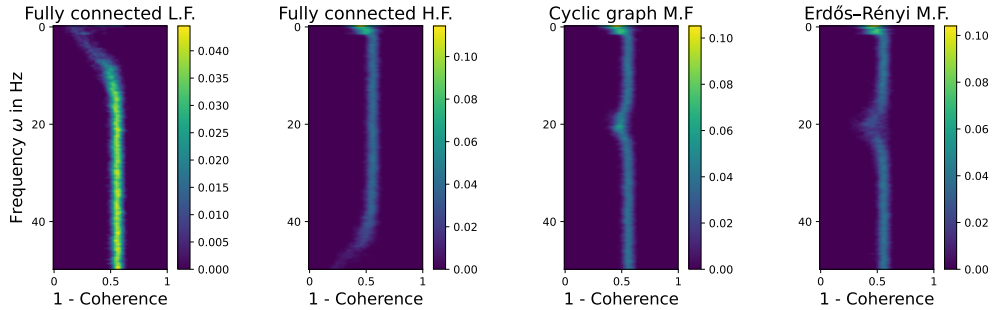


Figure 14: Left to right: Spectral landscape functions for settings 1–4 for the 1-dimensional homology.

The spectral landscapes (SL) for the 0-dimensional and the 1-dimensional homology groups seem to display differences and similarities at various frequency bands. From example, the averaged SLs for Settings 1 and 2 seem to be very similar at the middle frequencies but very different at both low and high frequencies for the 0-dimensional homology, see Figure 13. Conversely, for Settings 3 and 4, the averaged SLs seem to be very similar at all frequencies except at the middle frequencies around 20 Hertz, see Figures 13 and 14.

4.3 Pairwise testing at different frequency bands

In order to rigorously confirm the observations from the previous section we need to carry out formal statistical testing. For this reason, and following our approach presented in Section 3.4, we carried out a formal statistical test between all four settings. The results are reported in Tables 1 and 2, for both the 0-dimensional and 1-dimensional homology groups.

Table 1: Pairwise testing in Settings 1–4 across frequency bands using H_0 .

	Low freq: 0 to 12Hz				Middle freq: 12 to 27Hz				High freq: 27 to 50Hz			
	S_1	S_2	S_3	S_4	S_1	S_2	S_3	S_4	S_1	S_2	S_3	S_4
S_1	1	0	0	0	1	0	0	0	1	0	0.19	0.69
S_2	0	1	0.3	0.35	0	1	0	0	0	1	0	0
S_3	0	0.31	1	0.34	0	0	1	0	0.17	0	1	0.43
S_4	0	0.34	0.33	1	0	0	0	1	0.69	0	0.44	1

Table 2: Pairwise testing in Settings 1–4 across frequency bands using H_1 .

	Low freq: 0 to 12Hz				Middle freq: 12 to 27Hz				High freq: 27 to 50Hz			
	S_1	S_2	S_3	S_4	S_1	S_2	S_3	S_4	S_1	S_2	S_3	S_4
S_1	1	0	0	0	1	0	0	0	1	0	0.17	0.15
S_2	0	1	0.55	0.08	0	1	0	0	0	1	0	0
S_3	0	0.55	1	0.42	0	0	1	0	0.18	0	1	0.24
S_4	0	0.08	0.42	1	0	0	0	1	0.16	0	0.24	1

The (p^{th}, q^{th}) entry in the tables corresponds to the p-value resulting from pairwise testing between the p -th and q -th scenarios, using 0- and 1-dimensional Homology group information within the specified frequency bands. The derived p-values validate our visual observations and align with the simulation design. Notably, the first scenarios intentionally feature complete connectivity at either low or high frequency bands, while the last two scenarios exhibit distinct patterns within the beta frequency band.

5. Spectral Landscapes in EEGs: Controls vs ADHD

The goal in this section is to determine how mental diseases such as attention deficit hyperactivity disorder (ADHD) can alter the topology of brain functional connectivity networks in the young healthy control. Specifically, the impact of ADHD on the community structure of brain regions as described by the 0-dimensional homology and the holes in the brain connectivity as described by the 1-dimensional homology, across various frequency bands.

5.1 The data: From brain signals to spectral landscapes

The ADHD EEG data set Nasrabadi et al. (2020) consists of EEG recordings from 61 children diagnosed with ADHD and 60 healthy controls aged between 7 and 12 years old. The ADHD children were prescribed with the medication Ritalin for up to 6 months. None of the children in the control group had a history of psychiatric disorders, epilepsy, or any report of high-risk behaviors. EEG signals ((see Figures 15 and 16) were recorded based on 10-20 standard by 19 channels at a sampling frequency of 128 Hertz and were pre-processed using standard pipelines to remove artifacts (see below for more details). Among the deficits

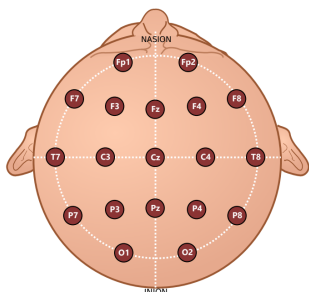


Figure 15: Scalp EEG, 10-20 standard layout.

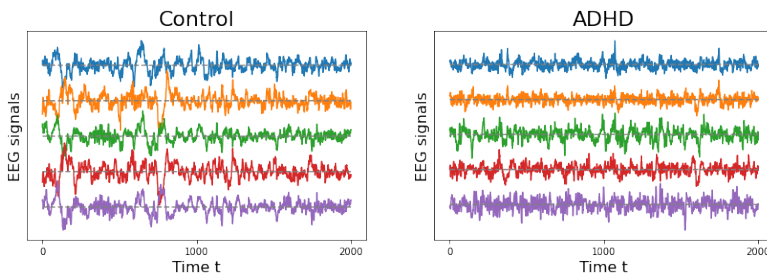


Figure 16: Example of observed EEG signals (five electrodes) from healthy controls and ADHD subjects.

of ADHD children is visual attention, therefore, the EEG recording protocol was based on a visual attention task. The children were shown a series of sets of characters and were asked to count the number of characters in a set flashed on the computer monitor. To ensure a continuous stimulus throughout the recording, each image was displayed immediately and uninterrupted after the child's response. Hence, the duration of EEG recording throughout this cognitive visual task was based on the speed of the child's response. Only data from 51 subjects with ADHD were kept, and 53 from the control group. The PREP pipeline (described in Nasrabadi et al. (2020)) was utilized for preprocessing. The steps included removal of the effect of the electrical line; removal of artifacts due to eye movements eye blinks or muscular movements; detection, removal (if necessary) and repair of bad quality channels; filtering of non-relevant signal components and finally re-referencing the signal to improve topographical localization.

After applying the pre-processing pipeline, the coherence matrices are estimated for the following frequency bands ($\delta = [0.5Hz, 4Hz]$, $\theta = [4Hz, 8Hz]$, $\alpha = [8Hz, 12Hz]$, $\beta = [12Hz, 30Hz]$ and $\gamma = [30Hz, 50Hz]$) and are used to build the distance function. For every frequency band, we constructed the spectral landscapes for: ADHD and healthy controls. See Figure 17 and 18 for the 0- and 1-dimensional homology groups, respectively. The advantage of using spectral landscapes - instead of persistence landscapes - is that it provides visualization of the topological changes in brain connectivity across the entire range of frequency bands. This enables us to develop a frequency-specific testing procedure for topological differences in brain dependence. Both Figures 17 and 18 display the frequency-

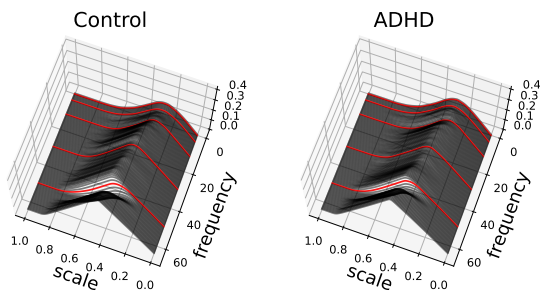


Figure 17: Estimated population mean spectral landscape for the 0-dimensional homology group. Left: control group. Right: ADHD group. The red lines delimit the various frequency bands.

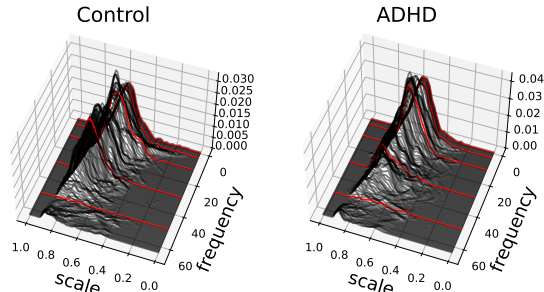


Figure 18: Estimated population mean spectral landscape for the 1-dimensional homology group. Left: control group. Right: ADHD group. The red lines delimit the various frequency bands.

specific features in the sample average spectral landscape. However, it remains unclear how to assess the statistical significance of such discrepancies between the brain topology of the two groups. Here, we develop a formal statistical inference for frequency-specific testing to compare both groups and assess the topological differences across different frequency bands.

5.2 Frequency-specific testing for topological differences

Given that the spectral landscapes $\Lambda_i(s, \omega)$ are two-dimensional functions for every homology dimension, we use the results derived in Section 3 to analyze the spectral landscapes of both control and ADHD groups.

5.2.1 EIGENDECOMPOSITION OF SPECTRAL LANDSCAPES

Based on Mercer’s theorem (Bartlett (2008)), we derive the eigendecomposition of the covariance function for the control group. Using Equation 8 to estimate the control group covariance function, we obtain the following eigenfunctions for both homology groups of dimension 0 and 1, see Figures 19 and 20.

Now applying Karhunen-Loève theorem leads to the following projections of the spectral landscapes onto the first four principal components, see Figures 21 and 22. From these figures, it becomes evident that the spectral landscapes encode crucial topological information pertaining to the organization of the human brain. Notably, an increase in the spectral landscape signifies the presence of significant topological features within the dependence network. For instance, when we observe an increase in the height of the H_1 surface at low frequencies, but not at high frequencies, this indicates the existence of cycles in the dependence network that are distinctly prevalent in the low-frequency range, while they are notably absent in the high-frequency domain.

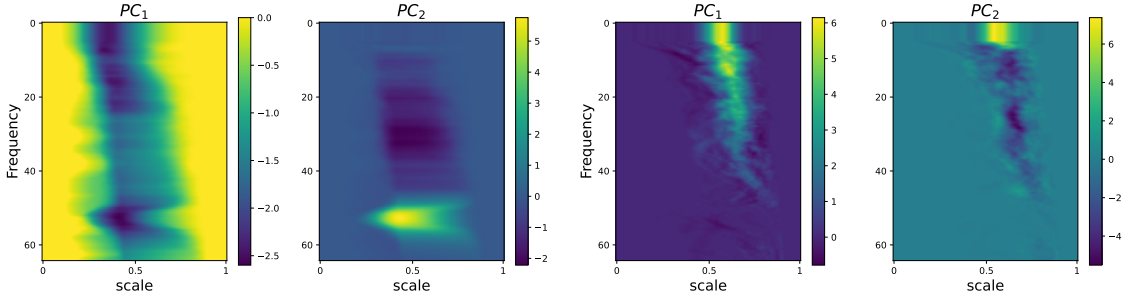


Figure 19: The first and second $(\hat{\phi}_1, \hat{\phi}_2)$ principal components or eigenfunctions for the 0-dimensional homology based on the control group spectral landscapes.

Figure 20: First two $(\hat{\phi}_1, \hat{\phi}_2)$ principal components or eigenfunctions for the 1-dimensional homology based on the control group spectral landscapes.

Similarly, variations observed in the H_0 surface reflect changes in the clustering patterns of the channels. In essence, the spectral landscapes serve as a visual representation of the intricate topological properties present in the brain’s functional connectivity. They allow us to discern and quantify the presence of specific topological features, such as cycles in the dependence network and channel clustering, shedding light on the nuanced organization of brain activity across different frequency bands. Regardless of how compelling these

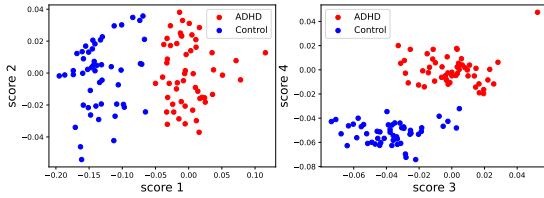


Figure 21: Scores of the eigendecomposition of the 0-dimensional spectral landscapes onto the first four principal components.

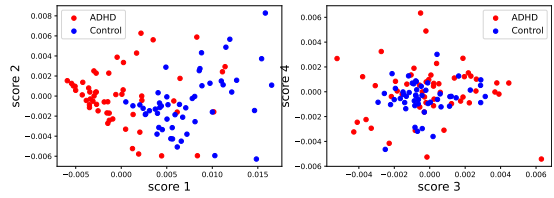


Figure 22: Scores of the eigendecomposition of the 1-dimensional spectral landscapes onto the first four principal components.

exploratory analytic results appear, it is necessary to carry out formal testing in order to assess the significance of such topological differences between the two groups.

Applying Theorem 6 in conjunction with Equation 15, we conduct an in-depth frequency-specific testing, see Figure 23, yielding novel insights. Our method effectively identifies significant topological alterations in brain clusters, notably within the gamma frequency band among ADHD subjects, affirming our findings at the 95% confidence level. These results enrich our understanding of brain dynamics and align with established literature.

Additionally, our examination uncovers notable topological changes in the cyclic dependence patterns, across the theta and gamma frequency bands, at the 95% confidence level. These discoveries, provide further insights into brain function and neurological disorders.

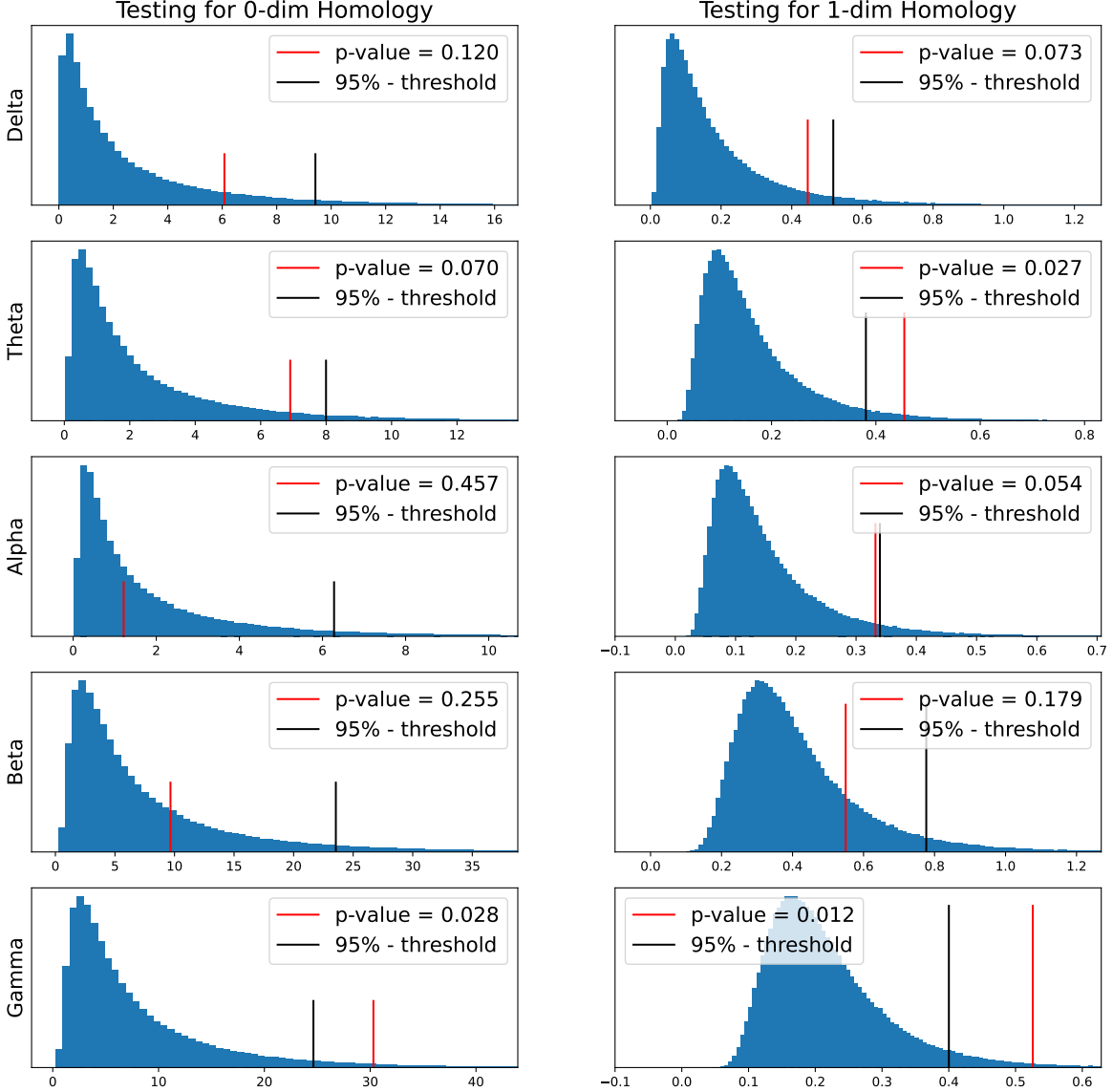


Figure 23: Frequency-specific test statistics $T_{N_1, N_2}^{\Omega_\ell}$ against the approximated threshold $\hat{\tau}_i$. Left: 0-dimensional spectral landscapes. Right: 1-dimensional spectral landscapes. Reference distribution in blue, 95-percentile in black, and observed test statistics in red with the corresponding p-values.

Our results from the proposed STDA method are particularly intriguing. Gamma rhythms are well-established as linked to cognitive functioning, learning, memory, and in-

formation processing, with their suppression potentially related to ADHD (Abhang et al. (2016)). In a similar vein, our findings present compelling evidence of statistically significant deviations in both clustering and cyclic structures within the organization of brain connectivity in ADHD children, compared to the control group.

6. Conclusion

In this paper, we have introduced a novel framework, namely STDA, for examining brain dependence networks in a frequency-specific manner. The novel notion of spectral landscape exhibits similar theoretical properties as the persistence landscape, such as the strong law of large numbers and the central limit theorem. By relying on coherence as a meaningful measure of connectivity, the spectral landscapes are capable of capturing the frequency-specific topological structure of brain networks, surpassing the limitations of traditional approaches based on correlations. In conjunction with coherence, we proposed the use of spectral landscapes, although our method is highly versatile and can be employed with various frequency-specific measures of dependence, thereby offering further insights into the topology of brain connectivity.

Furthermore, we have developed a frequency-specific statistical testing framework based on spectral landscapes and functional data analysis. The distribution of the test statistic has been provided, and we have implemented an asymptotically converging approximation. These advancements allow for rigorous statistical analysis of brain dependence networks in a frequency-specific context.

The observed alterations (in the clustering and cyclic dependence patterns) of the gamma rhythms in the brain activity of children diagnosed with ADHD offer valuable and novel insights into the complex mechanisms associated with this disorder. These findings shed light on the intricate neurological aspects of the ADHD and hold promise for further research.

Acknowledgments

The authors gratefully acknowledge financial support from the King Abdullah University of Science and Technology (KAUST) and Sarah Aracid (KAUST and University of the Philippines) for her invaluable help with the figures and artwork.

References

- Chapter 1 - an introduction to brain networks. In Alex Fornito, Andrew Zalesky, and Edward T. Bullmore, editors, *Fundamentals of Brain Network Analysis*, pages 1–35. Academic Press, San Diego, 2016. ISBN 978-0-12-407908-3. doi: <https://doi.org/10.1016/B978-0-12-407908-3.00001-7>.
- Priyanka A. Abhang, Bharti W. Gawali, and Suresh C. Mehrotra. Chapter 3 - technical aspects of brain rhythms and speech parameters. In *Introduction to EEG- and Speech-Based Emotion Recognition*, pages 51–79. Academic Press, 2016. ISBN 978-0-12-804490-2. doi: <https://doi.org/10.1016/B978-0-12-804490-2.00003-8>.

- T. Adamovich, I. Zakharov, A. Tabueva, et al. The thresholding problem and variability in the eeg graph network parameters. *Scientific Reports*, 12:18659, 2022. doi: 10.1038/s41598-022-22079-2.
- Henry Adams, Tegan Emerson, Michael Kirby, Rachel Neville, Chris Peterson, and Patrick Shipman. Persistence images: A stable vector representation of persistent homology. *Journal of Machine Learning Research*, 18:1–35, 2017. doi: <https://jmlr.org/papers/volume18/16-337/16-337.pdf>.
- Parinaz Babaeeghazvini, Laura M. Rueda-Delgado, Jolien Gooijers, Stephan P. Swinnen, and Andreas Daffertshofer. Brain structural and functional connectivity: A review of combined works of diffusion magnetic resonance imaging and electro-encephalography. *Frontiers in Human Neuroscience*, 15, 2021. doi: 10.3389/fnhum.2021.721206.
- Peter Bartlett. Reproducing kernel hilbert spaces. Lecture notes of CS281B/Stat241B Statistical Learning Theory, 2008. URL [URLwherethePDFcanbeaccessed](#). University of California at Berkeley.
- Danielle S. Bassett and Edward T. Bullmore. Small-world brain networks. *The Neuroscientist*, 12:512–523, 2006. doi: 10.1177/1073858406293182.
- Danielle S. Bassett and Edward T. Bullmore. Small-world brain networks revisited. *The Neuroscientist*, 23:499–516, 2017. doi: 10.1177/1073858416667720.
- Cécile Bordier, Carlo Nicolini, and Angelo Bifone. Graph analysis and modularity of brain functional connectivity networks: Searching for the optimal threshold. *Frontiers in Neuroscience*, 11, 2017. doi: 10.3389/fnins.2017.00441.
- Susan Bowyer. Coherence a measure of the brain networks: Past and present. *Neuropsychiatric Electrophysiology*, 2, 2016. doi: 10.1186/s40810-015-0015-7.
- Peter Bubenik. Statistical topological data analysis using persistence landscapes. *Journal of Machine Learning Research*, 16:77–102, 2015. doi: 10.5555/2789272.2789275.
- Edward Bullmore and Olaf Sporns. Complex brain networks: Graph theoretical analysis of structural and functional systems. *Nature reviews. Neuroscience*, 10:186–98, 2009. doi: 10.1038/nrn2575.
- Luigi Caputi, Anna Pidnebesna, and Jaroslav Hlinka. Promises and pitfalls of topological data analysis for brain connectivity analysis. *bioRxiv*, 2021. doi: 10.1101/2021.02.10.430469. URL <https://www.biorxiv.org/content/early/2021/02/11/2021.02.10.430469>.
- Gunnar Carlsson. Topology and data. *Bulletin of the American Mathematical Society*, 46: 255–308, 2009. doi: 10.1090/S0273-0979-09-01249-X.
- Gunnar Carlsson, Afra Zomorodian, Anne Collins, and Leonidas Guibas. Persistence barcodes for shapes. page 124–135. Association for Computing Machinery, 2004. doi: 10.1145/1057432.1057449.

- Eduarda Gervini Zampieri Centeno, Giulia Moreni, Chris Vriend, Linda Douw, and Fernando Antônio Nóbrega Santos. A hands-on tutorial on network and topological neuroscience. *Brain Structure and Function*, 227:741–762, 2022. doi: 10.1007/s00429-021-02435-0.
- M.P.van den Heuvel, C.J. Stam, M. Boersma, and H.E. Hulshoff Pol. Small-world and scale-free organization of voxel-based resting-state functional connectivity in the human brain. *NeuroImage*, 43:528–539, 2008. doi: <https://doi.org/10.1016/j.neuroimage.2008.08.010>.
- Herbert Edelsbrunner and John Harer. Persistent homology—a survey. *Discrete and Computational Geometry*, 453:257–282, 2008. doi: 10.1090/conm/453/08802.
- Herbert Edelsbrunner, David Letscher, and Afra Zomorodian. Topological persistence and simplification. 28:511–533, 2002. doi: doi.org/10.1007/s00454-002-2885-2.
- Anass B. El-Yaagoubi, Moo K. Chung, and Hernando Ombao. Modeling and simulating dependence in networks using topological data analysis. *arXiv*, 1:1, 2022. doi: 10.48550/arXiv.2209.10416.
- Anass B. El-Yaagoubi, Moo K. Chung, and Hernando Ombao. Topological data analysis for multivariate time series data. *Entropy*, 25:1509, 2023. doi: 10.3390/e25111509.
- Mark Fiecas and Hernando Ombao. Modeling the evolution of dynamic brain processes during an associative learning experiment. *Journal of the American Statistical Association*, 111:1440–1453, 2016. doi: 10.1080/01621459.2016.1165683.
- Karl J. Friston. Functional and effective connectivity: A review. *Brain Connectivity*, 1: 13–36, 2011. doi: 10.1089/brain.2011.0008.
- X. Gao, B. Shahbaba, N. Fortin, and H. Ombao. Evolutionary state-space models with applications to time-frequency analysis of local field potentials. *Statistica Sinica*, 30: 1561–1582, 2020. doi: 10.5705/ss.202017.0420.
- S. Gholizadeh and Wlodek Zadrozny. A short survey of topological data analysis in time series and systems analysis. *ArXiv*, abs/1809.10745, 2018.
- Robert Ghrist. Barcodes: The persistent topology of data. *Bulletin of the American Mathematical Society*, 45:61–75, 2008. doi: 10.1090/S0273-0979-07-01191-3.
- Gerald M. Edelman Giulio Tononi, Olaf Sporns. Reentry and the problem of integrating multiple cortical areas: simulation of dynamic integration in the visual system. *Cereb Cortex*, 2:310–35, 1992. doi: 10.1093/cercor/2.4.310.
- Chad Giusti, Eva Pastalkova, Carina Curto, and Vladimir Itskov. Clique topology reveals intrinsic geometric structure in neural correlations. *Proceedings of the National Academy of Sciences*, 112:13455–13460, 2015. doi: 10.1073/pnas.1506407112.
- G. Granados-Garcia, M. Fiecas, B. Shahbaba, N. Fortin, and H. Ombao. Modeling brain waves as a mixture of latent processes. *Computational Statistics and Data Analysis*, 174, 2022. doi: 10.1016/j.csda.2021.107409.

- Jean-Claude Hausmann. *On the Vietoris-Rips complexes and a Cohomology Theory for metric spaces*. Princeton University Press, 2016. doi: doi:10.1515/9781400882588-013.
- J. Hoffmann-Jørgensen and G. Pisier. The law of large numbers and the central limit theorem in banach spaces. *The Annals of Probability*, 4:587–599, 1976. doi: <https://www.jstor.org/stable/2243043>.
- Lajos Horváth and Piotr Kokoszka. *Inference for functional data with applications*, volume 200. Springer Science & Business Media, 2012.
- Nicolas Langer, Andreas Pedroni, and Lutz Jäncke. The problem of thresholding in small-world network analysis. *PloS one*, 8:e53199, 2013. doi: 10.1371/journal.pone.0053199.
- Michel Ledoux and Michel Talagrand. *Probability in Banach Spaces. Classics in Mathematics*. Springer-Verlag, Berlin, 2011. ISBN 978-3-642-20211-7.
- Hyekyoung Lee, Hyejin Kang, Moo K. Chung, Bung-Nyun Kim, and Dong Soo Lee. Persistent brain network homology from the perspective of dendrogram. *IEEE Transactions on Medical Imaging*, 31:2267–2277, 2012. doi: 10.1109/TMI.2012.2219590.
- Sergei Merkulov. Algebraic topology. *Proceedings of the Edinburgh Mathematical Society*, 46, 2003. doi: 10.1017/S0013091503214620.
- Francesca Miraglia, Fabrizio Vecchio, Chiara Pappalettera, Lorenzo Nucci, Maria Cotelli, Elda Judica, Florinda Ferreri, and Paolo Maria Rossini. Brain connectivity and graph theory analysis in alzheimer’s and parkinson’s disease: The contribution of electrophysiological techniques. *Brain Sciences*, 12:402, 2022. doi: 10.3390/brainsci12030402.
- James R. Munkres. *Elements of Algebraic Topology*. Addison Wesley Publishing Company, 1984. ISBN 9780429962462.
- Ali Nasrabadi, Armin Allahverdy, Mehdi Samavati, and Mohammad Reza Mohammadi. Eeg data for adhd / control children, 2020.
- Andrew Newman. A lower bound on the number of homotopy types of simplicial complexes on n vertices. *Combinatorica*, 42:1439–1450, 2022. doi: 10.1007/s00493-022-4877-6.
- Paul L. Nunez and Ramesh Srinivasan. *Electric Fields of the Brain: The neurophysics of EEG*. Oxford University Press, 2006. ISBN 9780195050387. doi: 10.1093/acprof:oso/9780195050387.001.0001.
- Hernando Ombao and Marco Pinto. Spectral dependence. *Econometrics and Statistics*, 2022. doi: <https://doi.org/10.1016/j.ecosta.2022.10.005>.
- Hernando Ombao and Sébastien Van Bellegem. Evolutionary coherence of nonstationary signals. *IEEE Transactions on Signal Processing*, 56:2259–2266, 2008. doi: 10.1109/TSP.2007.914341.
- Hernando Ombao, Rainer von Sachs, and Wensheng Guo. Slex analysis of multivariate nonstationary time series. *Journal of the American Statistical Association*, 100:519–531, 2005. doi: <https://doi.org/10.1198/016214504000001448>.

- Hae-Jeong Park and Karl Friston. Structural and functional brain networks: From connections to cognition. *Science*, 342:1238411, 2013. doi: 10.1126/science.1238411.
- T. Park, I. A. Eckley, and H. C. Ombao. Estimating time-evolving partial coherence between signals via multivariate locally stationary wavelet processes. *IEEE Transactions on Signal Processing*, 62:5240–5250, 2014. doi: 10.1109/TSP.2014.2343937.
- Jose A. Perea and John Harer. Sliding windows and persistence: An application of topological methods to signal analysis. *Foundations of Computational Mathematics*, 15:799–838, 2015. doi: 10.1007/s10208-014-9206-z.
- Charles Garrett Phillips, S. Zeki, and H. B. Barlow. Localization of function in the cerebral cortex. past, present and future. *Brain : a journal of neurology*, 107:327–61, 1984.
- John C. Shaw. Correlation and coherence analysis of the eeg: A selective tutorial review. *International Journal of Psychophysiology*, 1:255–266, 1984. doi: [https://doi.org/10.1016/0167-8760\(84\)90045-X](https://doi.org/10.1016/0167-8760(84)90045-X).
- Sean L. Simpson, F. DuBois Bowman, and Paul J. Laurienti. Analyzing complex functional brain networks: Fusing statistics and network science to understand the brain. *Statistics Surveys*, 7:1–36, 2013. doi: 10.1214/13-SS103.
- Olaf Sporns. *Networks of the Brain*. The MIT Press, 2010. doi: 10.7551/mitpress/8476.001.0001.
- Olaf Sporns. Graph theory methods: applications in brain networks. *Dialogues in Clinical Neuroscience*, 20:111–121, 2018. doi: 10.31887/DCNS.2018.20.2/osporns.
- Olaf Sporns, Giulio Tononi, and Rolf Kötter. The human connectome: A structural description of the human brain. *PLOS Computational Biology*, 1, 2005. doi: 10.1371/journal.pcbi.0010042.
- Y Wang, CM Ting, and H Ombao. Modeling effective connectivity in high dimensional source signals from eeg. *IEEE Journal of Selected Topics in Signal Processing*, 10:1315–1325, 2016.
- S Zeki, JD Watson, CJ Lueck, KJ Friston, C Kennard, and RS Frackowiak. A direct demonstration of functional specialization in human visual cortex. *Journal of Neuroscience*, 11: 641–649, 1991. doi: 10.1523/JNEUROSCI.11-03-00641.1991.